BCSJ

Selected Paper

Characteristics of Gelation by Amides Based on *trans*-1,2-Diaminocyclohexane: The Importance of Different Substituents

Haruka Nakagawa,[1] Mamoru Fujiki,[1] Takaaki Sato,[1] Masahiro Suzuki,[2] and Kenji Hanabusa*[2,3]

[1]Faculty of Textile Science & Technology, Shinshu University, Ueda, Nagano 386-8567

[2]Interdisciplinary Graduate School of Science & Technology, Shinshu University, Ueda, Nagano 386-8567

[3]Division of Frontier Fibers, Institute for Fiber Engineering, ICCER, Shinshu University, Ueda, Nagano 386-8567

E-mail: hanaken@shinshu-u.ac.jp

Received: October 28, 2016; Accepted: December 12, 2016; Web Released: February 25, 2017

Kenji Hanabusa

In 1979, Kenji Hanabusa started his academic carrier at Shinshu University as an Assistant Professor. He received Ph.D. from Osaka University in 1981 in Japan. In 1987, he was promoted to an Associate Professor, and since 1999, he has been a Full Professor in the Interdisciplinary Graduate School of Science and Technology at Shinshu University. His research interest is the development of low-molecular-weight gelators and thickeners on the basis of supramolecular chemistry. He has published more than 300 articles including original papers, reviews, and chapters of books.

Abstract

Six diamides were prepared from *trans*-(1*R*,2*R*)-1,2-diaminocyclohexane and the corresponding racemate and were subsequently used as gelators. Three chiral compounds and their racemates were prepared. One of the chiral compounds and its racemate contained two *n*-dodecanoylamino groups as the same substituents. The other two chiral compounds and their racemates contained different substituents: 10-undecenoylamino and 2-heptyl-undecanoylamino groups, and 5-hydroxypentanoylamino and 2-heptylundecanoylamino groups. Their gelation abilities were evaluated on the basis of the minimum gel concentration using eight solvents. The thermal stability and transparency of the gels were investigated by UV–vis spectroscopy using three-component mixed solvents of hexadecyl 2-ethylhexanoate, liquid paraffin, and decamethyl cyclopentasiloxane (66 combinations). The gel-to-sol phase-transition temperatures were also studied. The viscoelastic behavior of the gels was studied by rheology measurements in the strain sweep mode. Aggregates constructing three-dimensional networks were studied by transmission electron microscopy and circular dichroism spectroscopy. The molecular packing of the gels was evaluated by small angle X-ray scattering (SAXS).

1. Introduction

Recently, low-molecular-weight gelators have attracted special attention because large volumes of solvent can often be immobilized by very small amounts of such compounds. With advances in supramolecular chemistry, numerous reports on gelators have been published in recent years.[1–22] Another reason for researchers' interest in gelators lies in their potential industrial applications. Various compounds have been developed as gelators for use in cooking oils, spilled crude oil, cosmetics, aromatic compounds, ink thickeners, and greases. For example, 12-hydroxystearic acid[23] has been used practically as a gelator for cooking oil. As other examples, the (1,3:2,4)-dibenzylidenesorbitol[24] and the α,γ-bis-*n*-butylamide of *N*-lauroyl-L-glutamic acid are used in antiperspirants, and aromatic diureas are used in synthetic greases.

Physical gelation by low-molecular-weight compounds results from noncovalent bonds, such as hydrogen bonding, electrostatic interaction, van der Waals interaction, and π–π interaction. During a gelation process, gelator molecules are first self-assembled during a cooling process, producing fibrous assemblies. These fibrous assemblies form a three-dimensional network structure, and gelation occurs as solvent molecules are trapped in the network.

Physical gelation by a gelator can usually be best understood as resulting from competition between a gelator's tendency to dissolve via solvation and its tendency to self-assemble and crystallize. That is, gels formed by gelators are reasonably assumed to be metastable materials that are formed preceding crystallization. Despite recent advances, designing a gelator is a formidable challenge, if not impossible. An effective approach to prevent the transformation from a metastable gel to a crystalline state has not been developed yet. Several other questions associated with the design of gelators remain unanswered. For instance, why do gelators in fluids form metastable gels instead of thermally stable crystals and what are the necessary and sufficient requirements, if any, for designing gelators? Notably, most of the reported gelators have a chiral carbon center in their

structure, although exceptions are known.[25–30] We previously synthesized several types of gelators from chiral compounds and observed that the corresponding racemates tend to crystallize rather than form gels.[31–33] This behavior is explained by Wallach's rule;[34,35] specifically, racemic crystals tend to be denser than their chiral counterparts and the former is more stable than the latter. Despite racemic compounds being generally less expensive than chiral compounds, racemates are unfortunately unsuitable for use as gelators because of Wallach's rule. Resolving this apparent contradiction requires the development of a method to prevent the denser packing of molecules in racemates.

In the present paper, we focus on diamides derived from *trans*-1,2-diaminocyclohexane and study the effect of different substituents on the diamides' gelation abilities. We attached different substituents onto racemic *trans*-1,2-diaminocyclohexane with the expectation that the different substituents would prevent denser packing, resulting in physical gelation. The incorporation of different substituents may lead to new gelators if disordered molecular packing occurs.

2. Experimental

2.1 Instrumentation. Elemental analysis was performed with a Perkin-Elmer 240B analyzer. Infrared spectra were recorded on a Jasco FTIR-7300 spectrometer using KBr plate. UV–vis and CD spectra were recorded on a Jasco V-570UV/VIS/NIR and a Jasco J-600, respectively. Transmission electron microscopy (TEM) and field emission SEM (FE-SEM) were done with a JEOL JEM-SS and a Hitachi S-5000, respectively. Rheology was measured with an Elquest Rheologia A300.

2.2 Gelation Test. Gelation test was carried out by an upside-down test tube method. A typical procedure is as follows: A weighed sample and 1 mL of solvent in a septum-capped test tube with internal diameter of 14 mm was heated until the solid dissolved. The resulting solution was cooled at 25 °C for 2 h and then the gelation was checked visually. When no fluid ran down the wall of the test tube upon inversion of tube, we judged it to be gel. The gelation ability was evaluated by the minimum gel concentration of a gelator necessary for gelation at 25 °C. The unit is g L^{-1} (gelator/solvent). The solvents used for gelation test were ethyl acetate, isopropyl myristate, γ-butyrolactone, toluene, liquid paraffin, silicone oil (KF-54), decamethyl cyclopentasiloxane (D5), and hexadecyl 2-ethylhexanoate.

2.3 Synthesis. *trans*-(1*R*,2*R*)-(−)-1,2-Diaminocyclohexane and racemic *trans*-1,2-diaminocyclohexane were purchased from Tokyo Chemical Industry Co. Ltd.

2.3.1 *trans*-(1*R*,2*R*)-1-Boc-amino-2-aminocyclohexane:[36] The 800 mL of methanol containing 16.53 g (0.453 mol) of dry HCl was added dropwise to the solution of 51.78 g (0.453 mol) of *trans*-(1*R*,2*R*)-(−)-1,2-diaminocyclohexane in 80 mL of methanol for 2 h. After adding 50 mL of water, 98.97 g (0.453 mol) of di-*t*-butyl dicarbonate was added by portions for 1 h. The mixture was stirred for 2 h, and then methanol was removed. The residue was rinsed with 900 mL of ether and the insoluble matter was filtered off and dried. The crude product was dissolved in 800 mL of water and then extracted with a mixture of 500 mL of CH_2Cl_2 and 340 mL of 2 M NaOH. The organic layer was retained and treated with $MgSO_4$ and the solvent evaporated. Recrystallization from 900 mL of ligroin gave 67.87 g (70%) of *trans*-(1*R*,2*R*)-1-Boc-amino-2-aminocyclohexane. IR (KBr, cm^{-1}): 1695 (νC=O urethane), 1554 (δN-H amide II).

2.3.2 (*R*,*R*)-1: A solution of 34.07 g (0.159 mol) of *trans*-(1*R*,2*R*)-1-Boc-amino-2-aminocyclohexane and 26.1 mL (0.238 mol) of *N*-methylmorpholine in 300 mL of dry THF was cooled in an ice-water bath, and then 48.16 g (0.159 mol) of 2-heptylundecanoyl chloride was added drop-by-drop. The mixture was stirred for 1 h in an ice water bath, followed by 3 h at room temperature. A filtrate without NEt_3/HCl salt was evaporated and recrystallized from a mixture of 650 mL of ethyl acetate and 250 mL of hexane. Yield; 71.78 g (94%). IR (KBr, cm^{-1}): 1690 (νC=O urethane), 1644 (νC=O amide I), 1520 (δN-H amide II).

2.3.3 (*R*,*R*)-2: 130 mL of 25% HBr/AcOH was added to 34.07 g (0.159 mol) of **(*R*,*R*)-1** in 100 mL of acetic acid and stirred overnight. After completely removing HBr/AcOH, 400 mL of ether was added to the resulting oily product and cooled. The oil crystallized. Yield; 66.25 g (96%). IR (KBr, cm^{-1}): 1644 (νC=O amide I), 1525 (δN-H amide II).

2.3.4 (*R*,*R*)-C12C18: A solution of 2.00 g (4.33 mmol) of **(*R*,*R*)-2** and 0.88 g (8.67 mmol) of triethylamine in 60 mL of dry THF was cooled in an ice water bath, and then 1.04 g (4.77 mmol) of *n*-dodecanoyl chloride was added drop-by-drop. The mixture was stirred for 3 h at room temperature. 100 mL of water was added to the reaction mixture and a precipitate was filtered off and dried. Recrystallization from a mixture of 200 mL of ethyl acetate and 100 mL of hexane gave 2.18 g (89%) of the product. IR (KBr, cm^{-1}): 3282 (νN-H), 1635 (νC=O amide I), 1544 (δN-H amide II). Found: C 76.49 H 13.07, N 4.91%. Calcd for $C_{36}H_{70}N_2O_2$: C 76.81, H 12.53, N 4.98%. ^{1}H NMR (400 MHz, $CDCl_3$, TMS, 25 °C): δ = 5.95 (d, 1H, J = 6.52 Hz, NH-CO), 5.90 (d, 1H, J = 6.84 Hz, NH-CO), 3.59–3.70 (m, 2H, -NH-C*H*(CH_2)-C*H*(CH_2)-NH-), 1.72–2.12 (m, 7H, -CO-C*H*CH_2(CH_2)-, -CO-C*H*$_2$$CH_2$-, cyclohexane-C*H*$_2$-($CH_2$)$_2$-C*H*$_2$-), 1.24–1.59 (br, 50H, alkyl, cyclohexane-C*H*$_2$-C*H*$_2$-), 0.85–0.89 (m, 9H, -CH_2C*H*$_3$).

2.3.5 Racemic *trans*-1-Boc-amino-2-aminocyclohexane: This compound was prepared from racemic *trans*-1,2-diaminocylohexane by a similar procedure to that described above. Yield; 77%. IR (KBr, cm^{-1}): 1682 (νC=O urethane), 1517 (δN-H amide II). Found: C 61.68, H 10.73, N 13.16%. Calcd for $C_{11}H_{22}N_2O_2$: C 61.65, H 10.35, N 13.07%.

2.3.6 *rac*-1: This compound was prepared from racemic *trans*-1-Boc-amino-2-aminocylohexane by a similar procedure to that described in **(*R*,*R*)-1**. Yield; 93%. IR (KBr, cm^{-1}): 1696 (νC=O urethane), 1638 (νC=O amide I), 1528 (δN-H amide II). Found: C 72.71, H 12.0, N 5.79%. Calcd for $C_{29}H_{56}N_2O_3$: C 72.45, H 11.74, N 5.83%.

2.3.7 *rac*-2: This compound was prepared from ***rac*-1** by a procedure similar to that described in **(*R*,*R*)-2**. Yield; 94%. IR (KBr, cm^{-1}): 1644 (νC=O amide I), 1525 (δN-H amide II). Found: C 62.19 H 10.83, N 6.22%. Calcd for $C_{24}H_{49}N_2OBr$: C 62.45, H 10.70, N 6.07%.

2.3.8 *rac*-C12C18: This compound was prepared from ***rac*-2** by a similar procedure to that described in **(*R*,*R*)-C12C18**. Yield; 94%. IR (KBr, cm^{-1}): 3282 (νN-H) 1635 (νC=O amide I), 1544 (δN-H amide II). Found: C 76.50 H 12.77, N 5.01%.

Calcd for $C_{36}H_{70}N_2O_2$: C 76.81, H 12.53, N 4.98%. ^{1}H NMR (400 MHz, $CDCl_3$, TMS, 25 °C): δ = 6.03 (d, 1H, J = 6.56 Hz, NH-CO), 5.96 (d, 1H, J = 6.88 Hz, NH-CO), 3.59–3.69 (m, 2H, -NH-C*H*(CH_2)-C*H*(CH_2)-NH-), 1.72–2.12 (m, 7H, -CO-C*H*CH_2(CH_2)-, -CO-C$H_2$$CH_2$-, cyclohexane-C$H_2$-($CH_2$)$_2$-C$H_2$-), 1.24–1.59 (br, 50H, alkyl, cyclohexane-CH_2-CH_2-), 0.85–0.89 (m, 9H, -CH_2CH_3).

2.3.9 (*R*,*R*)-C5H18: A solution of 2.90 g (6.23 mmol) of **(*R*,*R*)-2** and 100 mL of dichloromethane was shaken with 100 mL of 4 M NaOH in a separating funnel. The organic layer was treated with $MgSO_4$ and evaporated. Recrystallization from 2 mL of ligroin gave 2.20 g (92%) of *trans*-(1*R*,2*R*)-1-amino-2-(2-heptylundecanoylamino)cyclohexane. To a solution of 1.50 g (3.94 mmol) of *trans*-(1*R*,2*R*)-1-amino-2-(2-heptylundecanoylamino)cyclohexane in 30 mL of dry THF, 0.423 mL (3.94 mmol) of δ-valerolactone was added and refluxed overnight. The precipitated matter after cooling the reaction mixture was filtered off and washed with hexane. Recrystallization from a mixture of 25 mL of ethyl acetate and 15 mL of hexane gave 1.63 g (86%) of **(*R*,*R*)-C5H18**. IR (KBr, cm^{-1}): 3407 (νO-H), 3283 (νN-H), 1635 (νC=O amide I), 1543 (δN-H amide II). Found: C 72.19, H 12.17, N 5.66%. Calcd for $C_{29}H_{56}N_2O_3$: C 72.45, H 11.74, N 5.83%.

2.3.10 *rac*-C5H18: This compound was prepared from racemic *trans*-1-amino-2-(2-heptylundecanoylamino)cyclohexane via ***rac*-2** by a similar procedure to that described above. Recrystallization from a mixture of 80 mL of acetone and 20 mL of methanol gave the product in a yield of 78%. IR (KBr, cm^{-1}): 3407 (νO-H), 3283 (νN-H), 1636 (νC=O amide I), 1543 (δN-H amide II). Found: C 72.69, H 12.29, N 5.83%. Calcd for $C_{29}H_{56}N_2O_3$: C 72.45, H 11.74, N 5.83%.

2.3.11 (*R*,*R*)-C12C12: A solution of 1.19 g (10.4 mmol) of *trans*-(1*R*,2*R*)-(−)-1,2-diaminocyclohexane and 2.11 g (20.9 mmol) of triethylamine in 300 mL of dry THF was cooled in an ice water bath, and then 4.57 g (20.9 mmol) of *n*-dodecanoyl chloride was added drop-by-drop. The mixture was stirred for 3 h at room temperature. 20 mL of acetone was added to the reaction mixture and a precipitate was filtered off and washed with water. Recrystallization from 100 mL of chloroform gave 4.20 g (92%) of the product. IR (KBr, cm^{-1}): 3283 (νN-H), 1639 (νC=O amide I), 1546 (δN-H amide II). Found: C 75.28, H 13.00, N 6.04%. Calcd for $C_{32}H_{62}N_2O_2$: C 75.26, H 12.21, N 5.85%. ^{1}H NMR (400 MHz, $CDCl_3$, TMS, 25 °C): δ = 5.88 (d, 2H, J = 6.56 Hz, NH-CO), 3.62–3.67 (m, 2H, -NH-C*H*(CH_2)-C*H*(CH_2)-NH-), 1.73–2.17 (m, 8H, -CO-CH_2-CH_2-, cyclohexane-CH_2-), 1.55–1.58 (m, 4H, -CO-CH_2-CH_2-), 1.15–1.35 (br, 36H, alkyl), 0.87 (t, 6H, J = 13.72, -CH_2CH_3).

2.3.12 *ra*-C12C12: This compound was prepared from racemic *trans*-1,2-diaminocyclohexane by a similar procedure to that described above. Yield; 84%. IR (KBr, cm^{-1}): 3300 (νN-H), 1636 (νC=O amide I), 1542 (δN-H amide II). Found: C 75.22, H 12.98, N 6.08%. Calcd for $C_{32}H_{62}N_2O_2$: C 75.26, H 12.21, N 5.85%. ^{1}H NMR (400 MHz, $CDCl_3$, TMS, 25 °C): δ = 5.91 (d, 2H, J = 6.52 Hz, NH-CO), 3.59–3.69 (m, 2H, -NH-C*H*(CH_2)-C*H*(CH_2)-NH-), 2.00–2.16 (m, 8H, -CO-CH_2-CH_2-, cyclohexane-CH_2-), 1.55–1.58 (m, 4H, -CO-CH_2-CH_2-), 1.19–1.44 (br, 36H, alkyl), 0.87 (t, 6H, J = 13.64, -CH_2CH_3).

2.4 SAXS. Small angle X-ray scattering was recorded on an Anton Paar SAXS. The accessible q-range was between 0.06 and 28 nm^{-1}. The preheated gel sample was poured into a cylindrical quartz cell having a diameter of 1 mm and the measurement was started after standing for 1 h. A line-shaped monochromatic primary beam (Cu Kα radiation, λ = 0.1542 nm) was irradiated to the gel samples and the solvent. The background contributions from capillary and solvent were corrected. Since the scattering intensity from the gel sample rapidly converged to that of the solvent in the high-q range of q > 10 nm^{-1}, we discuss the corrected scattering patterns of the gel samples observed in 0.06 < q/nm^{-1} < 10 in a practical manner. A model independent collimation correction was made by relying on the Lake algorithm.[37] The scattering intensity of the gel samples were finally obtained on an absolute scale by referring to the forward intensity of the secondary standard (water).[38]

3. Results and Discussion

3.1 Gelation Abilities. We prepared six diamides derived from *trans*-1,2-diaminocyclohexane, as shown in Scheme 1. The chiral species containing the different substituents—specifically, *trans*-(1*R*,2*R*)-1-(dodecanoylamino)-2-(2-heptylundecanoylamino)cyclohexane—is abbreviated as **(*R*,*R*)-C12C18**. The corresponding racemate, which was prepared from racemic *trans*-1,2-diaminocyclohexane, is abbreviated as ***rac*-C12C18**. The chiral compound containing 5-hydroxypentanoylamino and 2-heptylundecanoylamino groups is abbreviated as **(*R*,*R*)-C5H18**. The corresponding racemate is abbreviated as ***rac*-C5H18**. The chiral and racemate containing two *n*-dodecanoylamino groups as the same substituents are denoted as **(*R*,*R*)-C12C12** and ***rac*-C12C12**, respectively.

One objective of the present study is to develop gelators based on racemic *trans*-1,2-diaminocyclohexane, which is

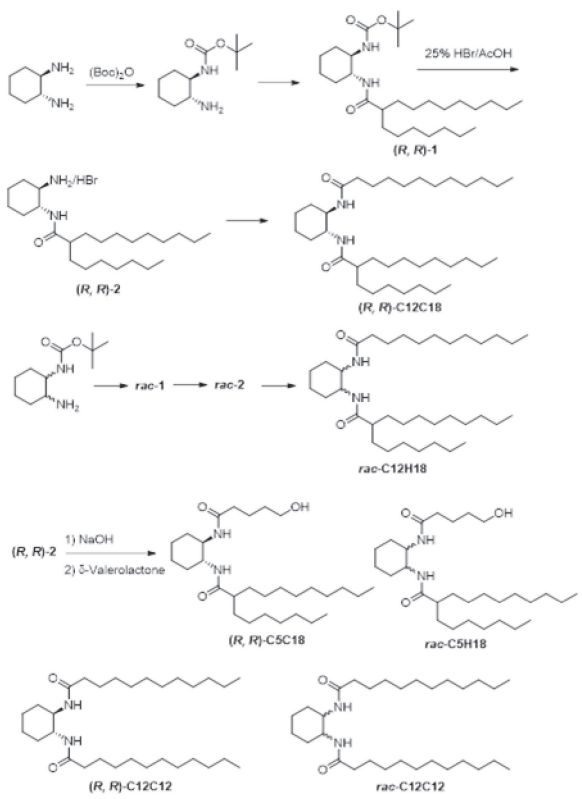

Scheme 1. Structures of gelators.

Table 1. Results of gelation tests at 25 °C

Solvent	(*R*,*R*)-C12C18	*rac*-C12C18	(*R*,*R*)-C5H18	*rac*-C5H18	(*R*,*R*)-C12C12	*rac*-C12C12
Ethyl acetate	GTL(8)	P	GTL(8)	P	GO(8)	GO(6)*
Isopropyl myristate	GTL(10)	GTL(20)	GTL(10)	GTL(4)	GTL(10)	P
γ-Butyrolactone	P	GT(40)	GTL(8)	GT(20)	GO(20)	P
Toluene	GT(40)	GT(40)	GT(40)	GT(20)	GT(12)	GT(20)*
Liquid paraffin	GT(4)	GTL(10)	GT(4)	GTL(8)	GT(3)	GTL(4)
Silicone oil (KF-54)	GTL(8)	GT(8)	GT(2)	GT(2)	GT(2)	GT(4)
D5	GTL(4)	GO(20)	GO(8)	GTL(4)	GO(2)	P
HDEH	GTL(8)	GTL(20)	GT(8)	GTL(8)	GTL(4)	GTL(8)*

GT: Transparent gel. GTL: Translucent gel. GO: Opaque gel. P: Precipitation. I: Almost insoluble. PG: Partial gel. KF-54: Poly(methylphenylsiloxane) of 400 cS. D5: Decamethyl cyclopentasiloxane. HDEH; Hexadecyl 2-ethylhexanoate. The values indicate the minimum gel concentrations at 25 °C; the units are g/l (gelator/solvent). *Crystals precipitated from the formed gels after several hours.

much less expensive than chiral *trans*-1,2-diaminocyclohexane. Because racemic compounds are unsuitable as gelators, as previously mentioned, the development of racemic gelators would represent an important advancement. Gelation tests were performed using an upside-down test-tube method. The macroscopic manifestation of successful gelation is the absence of observable flow when a sample is inverted. The results of the gelation tests with eight solvents are summarized in Table 1. Regarding **(*R*,*R*)-C12C12**, we have already reported its prominent gelation ability in a previous communication.[30] Notably, ***rac*-C12C12** could gel some of the solvents, but the formed gels were so unstable that crystallization occurred after several hours. In general, crystallization of a racemic mixture gives a racemic crystal comprising equivalent *R*- and *S*-configurations but does not result in precipitation of each chiral crystal separately. The facts that racemic crystals tend to be denser than their chiral counterparts and that complimentarily packing of *R*- and *S*-configurations gives more high-density crystals is known as Wallach's rule.[34,35] This rule is the reason that racemic mixtures are unsuitable as gelators.

New gelators **(*R*,*R*)-C12C18** and **(*R*,*R*)-C5H18** had high gelation abilities comparable to that of **(*R*,*R*)-C12C12**. Surprisingly, contrary to Wallach's rule, ***rac*-C12C18** and ***rac*-C5H18** formed very stable gels in isopropyl myristate, γ-butyrolactone, toluene, liquid paraffin, silicone oil (KF-54), decamethyl cyclopentasiloxane (D5), and hexadecyl 2-ethylhexanoate (HDEH), which were not transformed into crystals. The observation that ***rac*-C12C18** and ***rac*-C5H18** formed more stable gels than ***rac*-C12C12** can be explained on the basis of the disorder of molecular packing. The different substituents in ***rac*-C12C18** and ***rac*-C5H18** prevent the complimentarily denser packing; consequently, ***rac*-C12C18** and ***rac*-C5H18** are not precipitated as racemic crystals. The order of gelation ability to form stable gels is **(*R*,*R*)-C12C12** ≈ **(*R*,*R*)-C12C18** ≈ **(*R*,*R*)-C5H18** > ***rac*-C12C18** ≈ ***rac*-C5H18** ≫ ***rac*-C12C12**.

The gelation abilities of **(*R*,*R*)-C12C18**, **(*R*,*R*)-C5H18**, ***rac*-C12C18**, and ***rac*-C5H18** were investigated using three-component mixed solvents frequently used in cosmetics: HDEA as a polar oil, liquid paraffin as a non-polar oil, and D5 as a silicone oil. The concentrations of **(*R*,*R*)-C12C18**, ***rac*-C12C18**, **(*R*,*R*)-C5H18**, and ***rac*-C5H18** were fixed at 8, 10, 8, and 8 mg mL^{-1} (gelator/solvent), respectively. The gelation behavior of **(*R*,*R*)-C12C18** in the mixed solvent (66 combinations, with weight ratios ranging from 10:0:0 to 0:0:10 of HDEH, liquid paraffin, and D5) is shown in Figure 1. We observed that **(*R*,*R*)-C12C18** formed translucent gels with all these mixed solvent combinations. The same gelation behavior described in Figure 1 was observed for ***rac*-C12C18**, **(*R*,*R*)-C5H18**, and ***rac*-C5H18**.

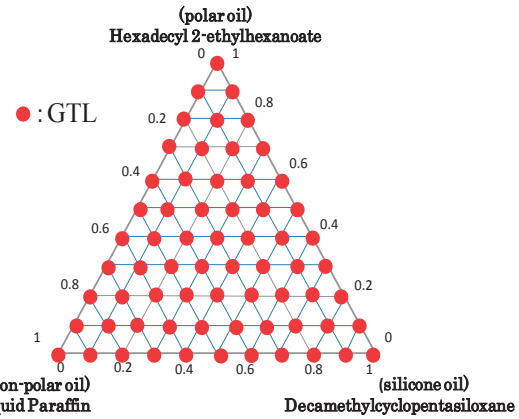

Figure 1. Gelation behavior of **(*R*,*R*)-C12C18** in the mixed solvent of HDEH, liquid paraffin, and D5 at concentration of 8 mg mL^{-1}.

The phase-transition temperatures of the prepared gels were investigated; the results are shown in Figure 2. As shown in Figure 2A, the greatest thermal stability was observed for gels formed by **(*R*,*R*)-C5H18**; their gel-to-sol phase-transition temperatures were within 95 to 115 °C. The second-most thermally stable gels were formed by ***rac*-C5H18**, as shown in Figure 2B. In the case of **(*R*,*R*)-C12C18**, when the content of HDED (polar oil) in the mixed solvents was increased, the phase-transition temperature which decreased from 65 °C to 74 °C is shown in Figure 2C. Figure 2D shows that the lowest phase-transition temperatures were observed in the gels formed by ***rac*-C12C18**. The high phase-transition temperatures of **(*R*,*R*)-C5H18** and ***rac*-C5H18** compared to those of **(*R*,*R*)-C12C18** and ***rac*-C12C18** is explained by the hydrogen bonding among hydroxyl groups. Although the reason of the low phase-transition temperatures of ***rac*-C12C18** compared to those of **(*R*,*R*)-C12C18** remains unclear, the enantiomer may prevent aggregate growth.

Transparent gels are widely desirable from a practical application perspective. We used UV–vis spectroscopy to evaluate the transparency of the prepared gels. As shown in Figure S1

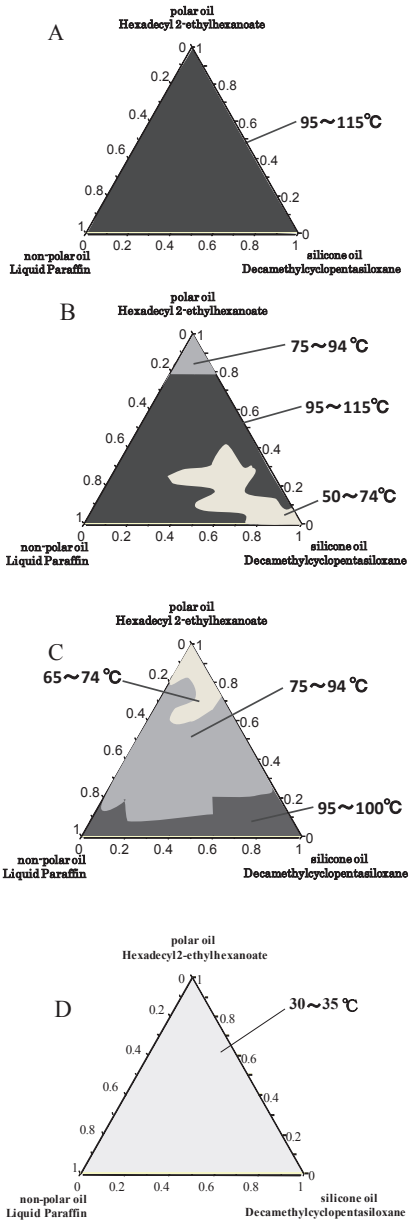

Figure 2. Gel-to-sol phase-transition temperatures in the mixed solvent of HDEH, liquid paraffin, and D5 at concentration of 8 mg mL^{-1}: (A) **(*R*,*R*)-C5C18**, (B) ***rac*-C5C18**, (C) **(*R*,*R*)-C12C18**, and (D) ***rac*-C12C18**.

the six gelators investigated in this work formed transparent or translucent gels. The transmittance spectra of gels composed of a mixture of HDEH, liquid paraffin, and D5 (vol. ratio 4:3:3) are shown in Figure 3. The transmittances at 400 nm of gels of **(*R*,*R*)-C12C18**, **(*R*,*R*)-C12C12**, **(*R*,*R*)-C5H18**, ***rac*-C12C18**, ***rac*-C12C12**, and ***rac*-C5C18** at a concentration of 10 mg mL^{-1} were 94, 79, 95, 58, 79, and 82%, respectively. The order of transparency of gels over the total investigated wavelength band is **(*R*,*R*)-C12C18** ≈ **(*R*,*R*)-C5H18** > **(*R*,*R*)-C12C12** ≈ ***rac*-C5H18** > ***rac*-C12C18** ≈ ***rac*-C12C12**. The transmittance of the ***rac*-C12C12** gel rapidly decreased because the gel crystallized. The transparency of gels is thought to depend on the size of the aggregates constructing the three-dimensional networks responsible for physical gelation. When the width of

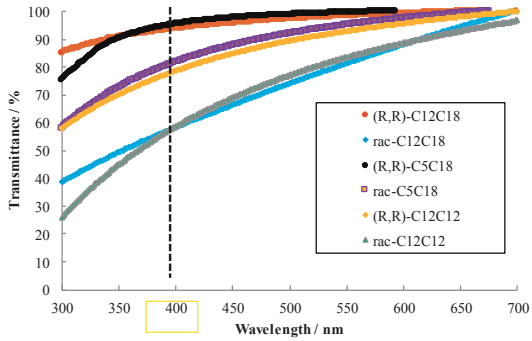

Figure 3. Transmittance change of gels at 10 mg mL^{-1} in the mixture of polar oil:non-polar oil:silicone oil = 4:3:3, as measured using a UV–vis spectrophotometer.

Table 2. G_{Ave}', G_{Ave}'', and tan δ_{Ave} under a strain of 0.02 at 25 °C

	G_{Ave}' (Pa)	G_{Ave}'' (Pa)	tan δ_{Ave}
(*R*,*R*)-C12C18	1455	303	0.20
***rac*-C12C18**	488	83	0.18
(*R*,*R*)-C5C18	2507	681	0.33
***rac*-C5C18**	1467	442	0.36
(*R*,*R*)-C12C12	1150	456	0.45
***rac*-C12C12**	857	291	0.38

the aggregates becomes equivalent to the wavelength of visible light, the formed gels will be opaque because they will scatter visible light. Because the disordered arrangements of structurally different substituents in **(*R*,*R*)-C12C18** and **(*R*,*R*)-C5H18** form aggregates with random molecular packing, the aggregates cannot grow to a size comparable to the wavelength of visible light. The different substituents in these compounds are thought to disturb the molecular packing. The introduction of structurally different substituents will be useful for developing gelators to form transparent gels.

3.2 Rheology. As shown in Figures S2–S4, the viscoelastic behavior of the gels was studied by rheology measurements in strain sweep mode and frequency sweep mode at 25 °C. The solvent used for the measurements was a mixture of HDEH, liquid paraffin, and D5 (vol. ratio 4:3:3) and the concentrations were 10 mg mL^{-1}. In strain sweep mode at 0.03 Hz, the storage elastic moduli (G') of almost all of the investigated gels were larger than the loss elastic moduli (G'') up to a strain of 0.1 and the G'' of the gels exceeded the G' at a strain of 0.5, which demonstrates the collapse of gels. In frequency sweep mode at a strain of 0.2, plateau regions of G' and G'' of all the samples were observed up to 1 Hz, where the G' exceeded the G''. In particular, the G' of **(*R*,*R*)-C12C18**, **(*R*,*R*)-C5H18**, and ***rac*-C5H18** exceeded the G'' up to 5 Hz. Average G' and G'' in the plateau regions of 0.002 to 1.0 Hz, referred to as G_{Ave}' and G_{Ave}'', and loss angle tan δ_{Ave} are summarized in Table 2, where the tangent of the phase angle (tan δ_{Ave})–the ratio of G_{Ave}'' to G_{Ave}' is a useful quantifier of the presence and extent of elasticity in a gel system.[39–41] The tan δ_{Ave} values of less than unity indicate elastic-dominant behavior and values greater than unity indicate viscous-dominant behavior. Regarding chiral compounds, the order of G_{Ave}' is **(*R*,*R*)-C12C12** < **(*R*,*R*)-C12C18** < **(*R*,*R*)-C5C18** and that of tan δ_{Ave} is **(*R*,*R*)-**

C12C12 > **(*R*,*R*)-C5C18** > **(*R*,*R*)-C12C18**. Namely, **(*R*,*R*)-C5C18** and **(*R*,*R*)-C12H18** with different substituents could form the harder gels. The hardness of gels seems to depend on size and density of aggregate; namely, the fibers consisting of the racemates are thicker than those of the enantiomers. For example, **(*R*,*R*)-C12C18** formed fine thread-like aggregates with nearly homogeneous diameters of ~26 nm, whereas the widths of fibers in ***rac*-C12C18** ranged from 42 to 50 nm. Results in SAXS stated later also suggests an importance of substituents; **(*R*,*R*)-C12C12** and ***rac*-C12C12** with the same substituent formed denser packed aggregates than **(*R*,*R*)-C12C18** and ***rac*-C12C18** with the different substituent. Because **(*R*,*R*)-C12C18** and **(*R*,*R*)-C5H18** with different substituents form fine aggregates, consequently, 3D networks in gels are crowded, and finally the hard gels are formed. The large G_{Ave}' of **(*R*,*R*)-C5H18**, compared to those of **(*R*,*R*)-C12H18**, will be attributed to the participation of hydrogen bonding among hydroxyl groups.

Next, we compared the behavior of the racemates; ***rac*-C12C12**, ***rac*-C12C18**, and ***rac*-C5H18**. Their behavior of G_{Ave}' is almost similar to that of chiral, i.e., the order of G_{Ave}' is ***rac*-C5C18** > ***rac*-C12C12** > ***rac*-C12C18**. G_{Ave}' and G_{Ave}'', and $\tan\delta_{Ave}$ of ***rac*-C5C18** were 1467 Pa, 442 Pa, and 0.36 respectively. Meanwhile, those of **(*R*,*R*)-C5H18** were 2507 Pa, 681 Pa, and 0.33 respectively. These results indicate that the gel strength of ***rac*-C5C18** was comparable to that of **(*R*,*R*)-C5C18**. The large G_{Ave}' of **(*R*,*R*)-C5H18** and ***rac*-C5H18** suggests that the hydrogen bonding among hydroxyl groups plays an important role in gelation.

3.3 TEM. The transparency and rheology behavior of the formed gels depended on the substituents and chirality of the gelators. Aggregates that formed three-dimensional networks consisting of gelator molecules were observed by TEM. Figure 4 shows TEM images of loose gels formed by **(*R*,*R*)-C12C18**, **rac-C12C18**, **(*R*,*R*)-C5C18**, **rac-C5C18**, **(*R*,*R*)-C12C12**, and ***rac*-C12C12**. The solvent was a mixture of HDEH, liquid paraffin, and D5 (vol. ratio 4:3:3). The concentrations of gelators for preparing samples were 0.5 mg mL^{-1} for **(*R*,*R*)-C12C18**, **rac-C12C18**, **(*R*,*R*)-C5C18**, and **rac-C5C18** and 0.8 mg mL^{-1} for **(*R*,*R*)-C12C12** and ***rac*-C12C12**. Because the concentrations of gelators used to prepare TEM samples were considerably lower than the minimum gel concentrations, the images in Figure 4 show fibers consisting of loose gels before actual gelation. The image of **(*R*,*R*)-C12C18** shows fine thread-like aggregates with nearly homogeneous diameters of ~26 nm. By contrast, the widths of fibers in ***rac*-C12C18** ranged from 42 to 50 nm, which is larger than the widths of the fibers in **(*R*,*R*)-C12C18**. The transparent gels formed by **(*R*,*R*)-C12C18** may be a consequence of the fine fibers. The widths of fibers of **(*R*,*R*)-C5C18** and ***rac*-C5C18** were ~20 nm and 30–58 nm, respectively. The fibers formed by the racemates are thicker than those formed by the enantiomers. The helicity of fibers of **(*R*,*R*)-C12C12** in acetonitrile was left-handed, as reported previously.[42] As shown in Figure S5, FE-SEM images also confirmed the left-handed helicity in the gels of toluene and isopropyl myristate. For reasons not clear to us, Figure 4A showed helical aggregates were not observed in gels formed by **(*R*,*R*)-C12C18**. The fibers of **(*R*,*R*)-C12C18** are so thin that they did not grow into helical aggregates that could be observed by TEM. Notably, as shown in Figure 4F, helical aggregates were observed in gels formed by ***rac*-C12C12**, although the helicity was unclear. We reasonably assume that the **(*R*,*R*)-C12C12** and *trans*-(1*S*,2*S*)-1,2-bis(dodecanoylamino)cyclohexane of the enantiomer included in ***rac*-C12C12** form helical fibers individually in the gel. However, this gel was unstable and crystallized via reconstitution of the enantiomers because of Wallach's rule.

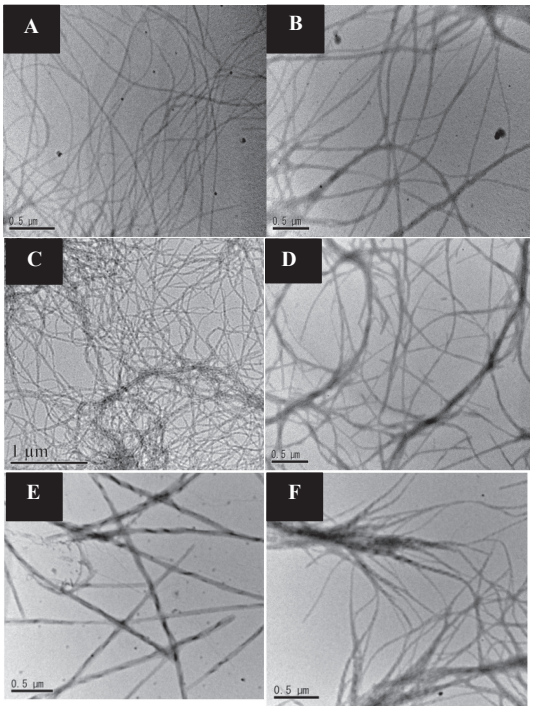

Figure 4. TEM images of gels prepared from (A) **(*R*,*R*)-C12C18** (0.5 mg mL^{-1}), (B) ***rac*-C12C18** (0.5 mg mL^{-1}), (C) **(*R*,*R*)-C5C18** (0.5 mg mL^{-1}), (D) ***rac*-C5C18** (0.5 mg mL^{-1}), (E) **(*R*,*R*)-C12C12** (0.8 mg mL^{-1}), and (F) ***rac*-C12C12** (0.8 mg mL^{-1}) in a mixture of polar oil:non-polar oil:silicone oil = 4:3:3.

To confirm the helical aggregates of **(*R*,*R*)-C12C18**, which we failed to detect in TEM and FE-SEM images, we recorded the gel's CD spectra. The solvent for CD spectroscopy was a mixture of HDEH, liquid paraffin, and D5 (vol. ratio; 4:3:3), and the concentration of **(*R*,*R*)-C12C18** in the prepared samples was 8 mg mL^{-1}. The CD spectrum of **(*R*,*R*)-C12C18** at 25 °C exhibited markedly strong peak for the amide unit: $[\theta]_{210}$ = ~50 mdeg. The intensity of this peak decreased with increasing temperature and disappeared at 50 °C because the loose gel was transformed into an isotropic solution. The disappearance of the CD signal in the isotropic solution led us to conclude that the strong CD band originates from helical aggregates of **(*R*,*R*)-C12C18** and not from the chirality of **(*R*,*R*)-C12C18** itself. The strong CD band supports the existence of helical aggregates in the gels of **(*R*,*R*)-C12C18**.

3.4 SAXS. The TEM observations suggested that the size and shape of aggregates in the gels depended on the type of substituents and the chirality of the gelators. To study the static structure of the aggregates in detail, we employed SAXS analyses. Figure 5 shows the SAXS intensities, $I(q)$, of dilute gel

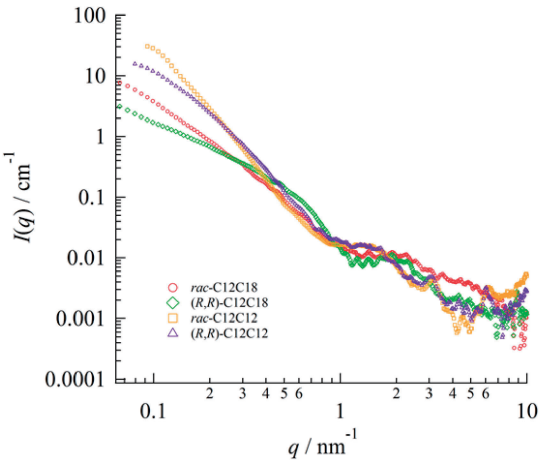

Figure 5. SAXS intensities, $I(q)$, of the gels prepared from ***rac*-C12C18**, **(*R*,*R*)-C12C18**, ***rac*-C12C12**, and **(*R*,*R*)-C12C12** at 10 mg mL^{-1} at 25 °C on an absolute scale. HDEH was used as the solvent.

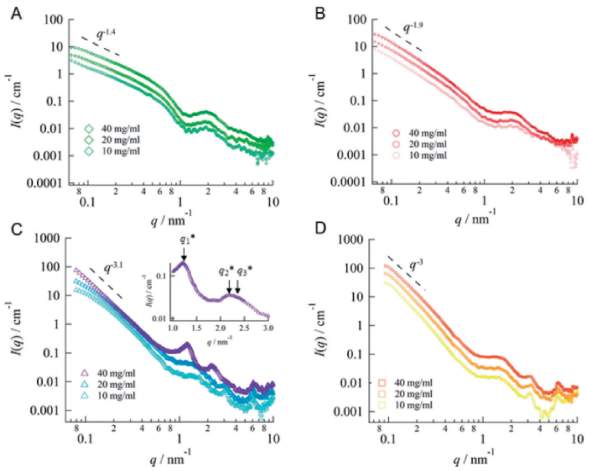

Figure 6. Concentration-dependence of the SAXS intensities $I(q)$ of gels at 25 °C in HDEH on an absolute scale. A; **(*R*,*R*)-C12C18**, B; ***rac*-C12C18**, C; **(*R*,*R*)-C12C12**, D; ***rac*-C12C18**.

samples prepared from **(*R*,*R*)-C12C18**, ***rac*-C12C18**, **(*R*,*R*)-C12C12**, and ***rac*-C12C12** at 25 °C on an absolute scale, where the solvent was HDEH and the concentration of the gelator was 10 mg mL^{-1}. The forward intensities of **(*R*,*R*)-C12C12** and ***rac*-C12C12** were significantly greater than those of ***rac*-C12C18** and **(*R*,*R*)-C12C18**, demonstrating that **(*R*,*R*)-C12C12** and ***rac*-C12C12** formed larger aggregates. We infer that **(*R*,*R*)-C12C12** and ***rac*-C12C12** form more densely packed aggregates than **(*R*,*R*)-C12C18** and ***rac*-C12C18**. The denser packing of **(*R*,*R*)-C12C12** and ***rac*-C12C12** appears to be a consequence of their ordered compact structures, because these gelators have the same substituents in their molecules, i.e., two *n*-dodecanoyl groups.

We next conducted a concentration series of SAXS experiments, and the results are demonstrated in Figure 6. Comparison of the $I(q)$ values of ***rac*-C12C12** and **(*R*,*R*)-C12C12** in the region $0.1 < q/\mathrm{nm}^{-1} < 1$ reveals that the $I(q)$ of ***rac*-C12C12** is nearly proportional to q^{-3}, regardless of the concentration. The greater forward intensities and the steeper slope of ***rac*-C12C12** compared to those of other systems demonstrated that this system forms larger aggregates than the other compounds. Because ***rac*-C12C12** has identical substituents in its molecules, it can easily achieve denser packing compared to other compounds with different substituents. In fact, ***rac*-C12C12**, comprising both the *R*- and *S*-configurations, tended to form high-density crystals due to Wallach's rule. The q^{-4} behavior is generally called the Porod scattering and is ascribed to interface formation. At low concentrations, such as 10 and 20 mg mL^{-1}, the slope of the $I(q)$ of **(*R*,*R*)-C12C12** in the forward direction was still gentler than q^{-4}, indicating that, even at 40 mg mL^{-1}, the aggregation tendency of the gelator was not strong enough to form a well-defined interface between the solvent and the fiber bundle-like higher-order aggregates.

The slope of the $I(q)$ of **(*R*,*R*)-C12C18** and ***rac*-C12C18** in the region $0.1 < q/\mathrm{nm}^{-1} < 1$ was virtually independent of the concentration. Generally, the fractal dimension of the scattering object, d_f, is manifested in the asymptotic exponent as $I(q) \propto q^{-df}$.[43] The asymptotic behavior of $I(q) \propto q^{-1}$ and $I(q) \propto q^{-2}$ in the forward direction can be assigned to rod and planar structures, respectively. As for **(*R*,*R*)-C12C18**, we observed a slope of $q^{-1.4}$ for $q < 0.3\ \mathrm{nm}^{-1}$ instead of q^{-1}, which implied the formation of aggregating rods. A steeper slope of $q^{-1.9}$ was observed for ***rac*-C12C18**, which was still slightly gentler than but close to q^{-2}, which may be assigned to a planar-like structure or alternatively an aggregating rod structure. If the gelling systems at low gelator concentrations can be regarded as a dilute dispersion of colloidal particles, $I(q)$ may be interpreted as the Fourier transformation of the pair-distance distribution function, $p(r)$, as given by

$$I(q) = 4\pi \int_0^\infty p(r) \frac{\sin qr}{qr} \mathrm{d}r \qquad (1)^{44,45}$$

To obtain $p(r)$ corresponding to the structure function in real space, we performed Fourier inversion analyses of the SAXS intensities $I(q)$ of **(*R*,*R*)-C12C18** and ***rac*-C12C18** at 40 mg mL^{-1}. First, we used an indirect Fourier transformation (IFT) technique,[46,47] assuming an isotropic dilute dispersion. The IFT fits to the experimental $I(q)$ and the resulting $p(r)$ values are displayed in Figure 7. As shown in Figure 7B, the deduced $p(r)$ of **(*R*,*R*)-C12C18** exhibits typical features of a rod-like structure, namely a local maximum in the low-r regime and an extended tail in the high-r regime. The maximum length, exceeding 50 nm, and the cross-sectional diameter, about 6 nm, can be determined from the maximum distance, where $p(r)$ approaches zero and the infraction point of $p(r)$ is seen on the slightly higher-r side of the local maximum. The latter is highlighted by an arrow and a dotted line in Figure 7B. Importantly, we simultaneously observed the emergence of a second additional local maximum at $r \approx 13$ nm, as indicated by a dotted arrow. Note that this behavior is quite similar to that observed for the $p(r)$ of the aggregating rod-like normal and reverse micelles in aqueous[48] as well as lipophilic[49] solvent conditions. The ***rac*-C12C18** system showed a more pronounced second local maximum, which is overwhelming and appears to hinder the first local maximum. Strongly linked with the $q^{-1.9}$ slope of the forward intensity, the $p(r)$ of ***rac*-C12C18**, at a glance, resembles that of a planar structure, rather

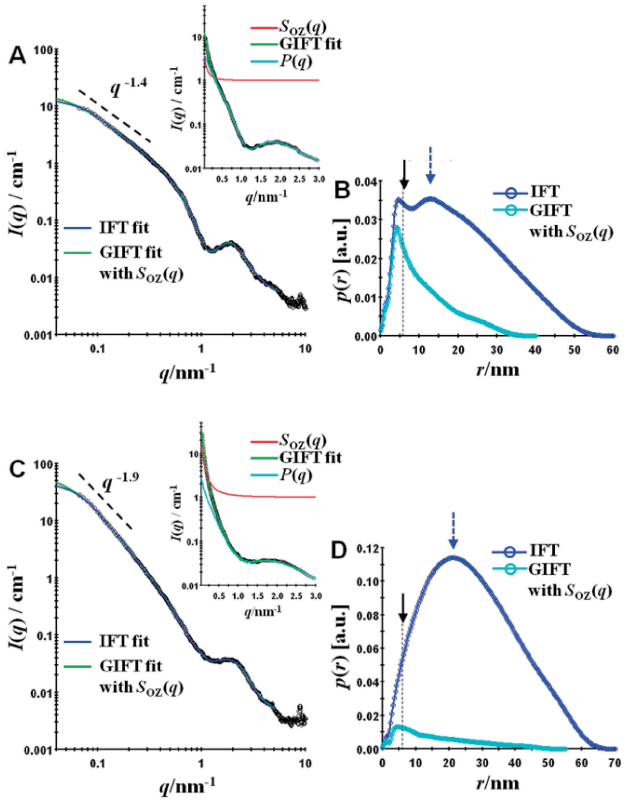

Figure 7. Fourier inversion analyses of SAXS intensities of **(*R*,*R*)-C12C18** (A and B) and ***rac*-C12C18** (C and D) gels (40 mg mL^{-1}) at 25 °C using IFT/GIFT technique. The IFT and GIFT fit results respectively without and with the Ornstein–Zernike structure factor model (A and C) and the resulting pair-distance distribution functions, $p(r)$ (B and D).

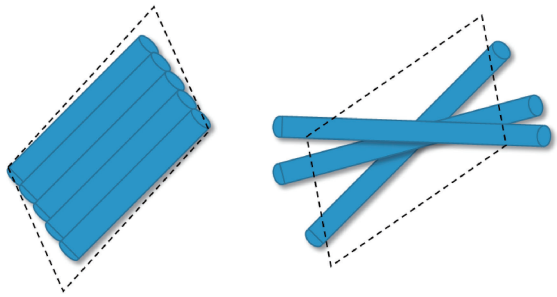

Figure 8. Schematic diagram of two structures discussed about ***rac*-C12C18**. Planer structure (left) and planer-like aggregates by aggregated-rods (right).

than that of a rod structure. However, we point out that the aggregating rods, closely positioned with a small mutual tilt angle, say less than 30°, can mimic the $p(r)$ of a planar-like structure; see Figure 8 or the literature.[43]

We tried to further confirm the above-mentioned IFT results and verify the aggregating rod-like structures in a more quantitative manner. An alternative interpretation of the enhanced forward scattering, i.e., $I(q) \propto q^{-1.4}$ for **(*R*,*R*)-C12C18** and $I(q) \propto q^{-1.9}$ for ***rac*-C12C18**, could be a critical-like concentration fluctuation due to the attractive interaction between the rod-like aggregates and the resulting upturn increase of the structure factor in the low-q region ($S(q) > 1$). We used a generalized indirect Fourier transformation (GIFT) technique,[50,51] taking the local concentration fluctuations into account. For the gel systems, we assumed a relation describing a concentrated colloidal dispersion, $I(q) = nP(q)S_{OZ}(q)$, where $P(q)$ is the form factor of the primary rod-like aggregates and $S_{OZ}(q)$ is a modified Ornstein–Zernike (OZ) structure factor, in which $S_{OZ}(q)$ is approximated by a Lorentzian function:

$$S_{OZ}(q) = 1 + \frac{nk_BT\chi_T}{1 + q^2\xi^2} \quad (2)$$

where k_B is the Boltzmann constant, T is the absolute temperature, ξ is the correlation length describing the length scale of the local concentration fluctuations, n is the particle number density, and χ_T is the isothermal osmotic compressibility. We treated ξ and the amplitude, $nk_BT\chi_T$, as the variable parameters, which grow when approaching the critical point.[52,53] In general, the OZ structure factor model is applied to the description of a temperature-induced critical fluctuation.[43] In this study, we used the same model for the gelling systems in an extended manner. As shown in Figure 7, the GIFT results demonstrated that the experimental $I(q)$ can be excellently reproduced by the product of $P(q)$, having the overall shape of the rod-like particles and $S_{OZ}(q)$ with the optimized parameters, yielding typical shapes of $p(r)$ for the long rod structure, having a cross-sectional diameter of about 6 nm for both **(*R*,*R*)-C12C18** and ***rac*-C12C18**. We obtained $\xi = 8$ nm and $nk_BT\chi_T = 2$ for **(*R*,*R*)-C12C18** and $\xi = 25$ nm and $nk_BT\chi_T = 5$ for ***rac*-C12C18**, indicating a larger concentration fluctuation for ***rac*-C12C18**. The difference in structural morphogenesis between **(*R*,*R*)-C12C18** and ***rac*-C12C18** can be explained by the existence of equimolar **(*S*,*S*)-C12C18** in ***rac*-C12C18**. The complimentarily packing of *R*- and *S*-configurations in ***rac*-C12C18** gives more high-density crystals, according to Wallach's rule. The IFT/GIFT results for these two gel systems led us to conclude that the presence of a long rod-like or strand structure is most likely and that these were aggregated to some extent in an aligned manner, but did not form a crystalline-like structure.

As we already discussed, neither a change in the position of the local maximum, nor a change in the slope of $I(q)$ was observed for **(*R*,*R*)-C12C18** and ***rac*-C12C18** with increasing concentration, as shown in Figures 7A and 7B. By contrast, with increasing concentration of **(*R*,*R*)-C12C12** and ***rac*-C12C12**, an interference peak (q_h) at about 6 nm^{-1} appeared, corresponding to a d-spacing of ~1 nm if Bragg's law was applied to q_h. Judging from the fact that the $q_h \approx 6$ nm^{-1} condition did not change with concentration, the peak appears to be attributed to the short distance between gelator molecules within the aggregates. Broad peaks of **(*R*,*R*)-C12C12** and ***rac*-C12C12** in the region $1 < q/\text{nm}^{-1} < 5$ are derived from the internal structure of the primary aggregates, which are likely to have a rod-like structure, thus do not exhibit inter-aggregate interference scattering. Similar broad peaks of **(*R*,*R*)-C12C18** and ***rac*-C12C18** observed in the region $1 < q/\text{nm}^{-1} < 4$ are also ascribed to the intra-aggregate interference contributions. However, when the concentration of **(*R*,*R*)-C12C12** was increased to 40 mg mL^{-1}, sharp interference peaks suddenly appeared in the

Table 3. SAXS diffraction peak data[a)]

Compound	q_1* (nm^{-1})	q_2* (nm^{-1})	q_3* (nm^{-1})	q_h (nm^{-1})	q_1*:q_2*:q_3*	d_1 (nm)	d_h (nm)
(*R*,*R*)-C12C12	1.21	2.20	2.41	6.17	1:√3:√4	5.19	1.02
***rac*-C12C12**	—	—	—	6.00	—	—	1.05

a) The scattering vectors corresponding to the position of the characteristic reflections q_n* ($n = 1, 2, \cdots$) and the interlayer spacing d are determined from the SAXS intensities. The interlayer spacing d is calculated using Bragg's law, $d_n = 2\pi/q_n$*.

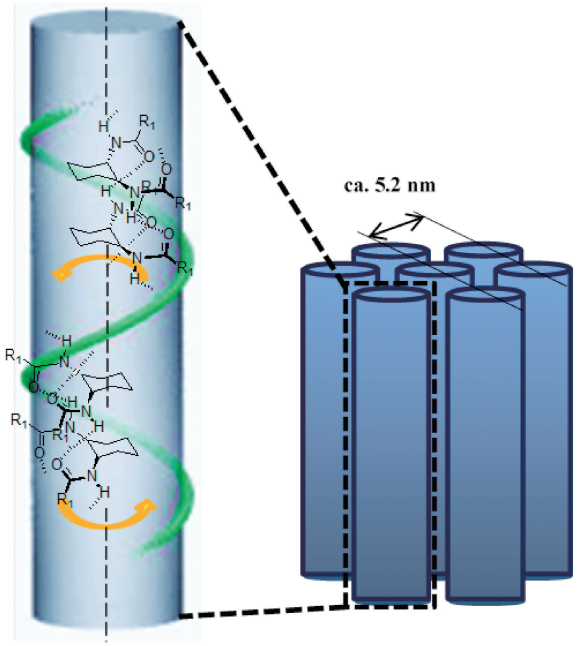

Figure 9. Organogel structure of **(*R*,*R*)-C12C12** with higher-order aggregates formed in hexadecyl 2-ethylhexanoate.

region $0.9 < q/\mathrm{nm}^{-1} < 4$, as shown in Figure 7C, which are likely to be interference peaks arising from the crystalline-like positional correlations of the aggregates. The interlayer spacing, d, values for **(*R*,*R*)-C12C12** and ***rac*-C12C12**, calculated from the interference peak positions, are summarized in Table 3. As previously mentioned, only in the case of **(*R*,*R*)-C12C12**, the forward intensity approached Porod scattering, and sharp peaks suddenly appeared at 40 mg mL^{-1}, which we call the scattering vectors corresponding to the peak positions q_1* and q_2* from the lower q-side. As shown in Figure 7C, the third reflection (q_3*) could also be vaguely identified. Since the positional ratio q_1*:q_2*:q_3* was nearly 1:√3:√4, the packing of the aggregates of **(*R*,*R*)-C12C12** at 40 mg mL^{-1} can be assigned to a hexagonal structure.[54] As shown in Figure 9, we can conclude that **(*R*,*R*)-C12C12** formed rod-like aggregates at low concentrations of 10 and 20 mg mL^{-1}, which then transformed into hexagonal aggregates at 40 mg mL^{-1}.

From the results showing that the forward scattering intensities of **(*R*,*R*)-C12C18** and ***rac*-C12C18** are smaller than those of **(*R*,*R*)-C12C12** and ***rac*-C12C12**, and moreover, the absence of interference peaks in **(*R*,*R*)-C12C18** and ***rac*-C12C18**, we can conclude that the different substituents in **(*R*,*R*)-C12C18** and ***rac*-C12C18** moderate the denser packing. Consequently, excessive aggregation is hindered in small aggregates.

4. Conclusion

We prepared three gelators, each of chiral and racemic types, based on *trans*-1,2-diaminocyclohexane. One is chiral and racemate containing *n*-dodecanoylamino groups as the same substituents. The others are chiral and racemates containing structurally different substituents: 10-undecenoylamino and 2-heptylundecanoylamino groups as the substituents in one case, and 5-hydroxypentanoylamino and 2-heptylundecanoylamino as the substituents in the other case. Results of gelation tests with eight solvents demonstrated that the order of gelation ability to form stable gels is **(*R*,*R*)-C12C12** ≈ **(*R*,*R*)-C12C18** ≈ **(*R*,*R*)-C5H18** > ***rac*-C12C18** ≈ ***rac*-C5H18** ≫ ***rac*-C12C12**. Although the gels formed by ***rac*-C12C12** were so unstable that they crystallized after several hours, both ***rac*-C12C18** and ***rac*-C5H18**, which included different substituents, formed very stable gels. The gelation abilities were investigated using three-component mixed solvents of HDEH, liquid paraffin, and D5 (66 combinations). **(*R*,*R*)-C12C18**, **(*R*,*R*)-C5H18**, ***rac*-C12C18**, and ***rac*-C5H18** all formed translucent gels with all of the investigated mixed solvent combinations. The thermal stabilities of the gels were evaluated on the basis of their phase-transition temperatures. The highest thermal stability was observed for gels formed by **(*R*,*R*)-C5H18**, and the second-most thermally stable gels were formed by ***rac*-C5H18**. The transmittance of gels composed of a mixture of HDEH, liquid paraffin, and D5 was studied. The order of transparency of gels over the total investigated wavelength band was **(*R*,*R*)-C12C18** ≈ **(*R*,*R*)-C5H18** > **(*R*,*R*)-C12C12** ≈ ***rac*-C5H18** > ***rac*-C12C18** ≈ ***rac*-C12C12**. The viscoelastic behavior of gels of a three-component mixed solvent was studied via rheology measurements. The **(*R*,*R*)-C5C18** and **(*R*,*R*)-C12H18** with different substituents formed the harder gels compared with **(*R*,*R*)-C12C12**. Electron microscopy images of **(*R*,*R*)-C12C18** showed fine thread-like aggregates with nearly homogeneous ~26 nm diameters. The widths of fibers of ***rac*-C12C18** ranged from 42 to 50 nm. The fibers formed by racemates were thicker than those formed by enantiomers. The left-handed helicity was confirmed in the gels formed by toluene and isopropyl myristate in **(*R*,*R*)-C12C12**. Helical aggregates in gels formed by **(*R*,*R*)-C12C18** were not observed by TEM; however, the appearance of a strong CD band supported the existence of helical aggregates in the gels. The IFT/GIFT results for **(*R*,*R*)-C12C18** and ***rac*-C12C18** indicate that the presence of a long rod-like or strand structure is most likely and that these were aggregated to some extent in an aligned manner, but not a crystalline-like structure. **(*R*,*R*)-C12C12** formed rod-like aggregates at low concentrations, which then transformed into hexagonal aggregates at 40 mg mL^{-1}. The forward scattering intensities of **(*R*,*R*)-C12C18** and ***rac*-C12C18** demonstrated

that the different substituents in **(*R*,*R*)-C12C18** and ***rac*-C12C18** moderate the denser packing. The restrain of excessive aggregation results in small aggregates. Finally, we clarified the importance of different substituents in diamides based on racemic *trans*-1,2-diaminocyclohexane on physical gelation. A concept of beingness of structurally different substituents will be helpful in development and molecular design of new gelators.

The present research was supported in part by JSPS KAKENHI Grant Number JP15K05623.

Supporting Information

Figure S1, Figure S2, Figure S3, Figure S4, and Figure S5. This material is available on http://dx.doi.org/10.1246/bcsj.20160360.

References

1 P. Terech, R. G. Weiss, *Chem. Rev.* **1997**, *97*, 3133.
2 J. H. van Esch, B. L. Feringa, *Angew. Chem., Int. Ed.* **2000**, *39*, 2263.
3 L. A. Estroff, A. D. Hamilton, *Chem. Rev.* **2004**, *104*, 1201.
4 P. Dastidar, *Chem. Soc. Rev.* **2008**, *37*, 2699.
5 V. K. Praveen, S. S. Babu, C. Vijayakumar, R. Varghese, A. Ajayaghosh, *Bull. Chem. Soc. Jpn.* **2008**, *81*, 1196.
6 S. Banerjee, R. K. Das, U. Maitra, *J. Mater. Chem.* **2009**, *19*, 6649.
7 M. Suzuki, K. Hanabusa, *Chem. Soc. Rev.* **2009**, *38*, 967.
8 M. Suzuki, K. Hanabusa, *Chem. Soc. Rev.* **2010**, *39*, 455.
9 J.-L. Li, X.-Y. Liu, *Adv. Funct. Mater.* **2010**, *20*, 3196.
10 G. John, B. V. Shankar, S. R. Jadhav, P. K. Vemula, *Langmuir* **2010**, *26*, 17843.
11 H. Svobodová, V. Noponen, E. Kolehmainen, E. Sievänen, *RSC Adv.* **2012**, *2*, 4985.
12 S. S. Babu, S. Prasanthkumar, A. Ajayaghosh, *Angew. Chem., Int. Ed.* **2012**, *51*, 1766.
13 A. Y.-Y. Tam, V. W.-W. Yam, *Chem. Soc. Rev.* **2013**, *42*, 1540.
14 J. Raeburn, A. Z. Cardoso, D. J. Adams, *Chem. Soc. Rev.* **2013**, *42*, 5143.
15 G. Yu, X. Yan, C. Han, F. Huang, *Chem. Soc. Rev.* **2013**, *42*, 6697.
16 M. D. Segarra-Maset, V. J. Nebot, J. F. Miravet, B. Escuder, *Chem. Soc. Rev.* **2013**, *42*, 7086.
17 S. S. Babu, V. K. Praveen, A. Ajayaghosh, *Chem. Rev.* **2014**, *114*, 1973.
18 D. K. Kumar, J. W. Steed, *Chem. Soc. Rev.* **2014**, *43*, 2080.
19 V. K. Praveen, C. Ranjith, N. Armaroli, *Angew. Chem., Int. Ed.* **2014**, *53*, 365.
20 M. Liu, L. Zhang, T. Wang, *Chem. Rev.* **2015**, *115*, 7304.
21 Y. Lan, M. G. Corradini, R. G. Weiss, S. R. Raghavan, M. A. Rogers, *Chem. Soc. Rev.* **2015**, *44*, 6035.
22 *Low Molecular Mass Gelators: Design, Self-Assembly, Function*, ed. by F. Fages, Springer, Berlin, Heidelberg, New York, **2005**. doi:10.1007/b105250.
23 T. Tachibana, T. Mori, K. Hori, *Bull. Chem. Soc. Jpn.* **1980**, *53*, 1714.
24 S. Yamamoto, *J. Chem. Soc. Jpn. Ind. Chem. Soc.* **1943**, *46*, 779; S. Yamamoto, *Chem. Abstr.* **1952**, *46*, 7047i.
25 F. Placin, M. Colomès, J.-P. Desvergne, *Tetrahedron Lett.* **1997**, *38*, 2665.
26 L. Lu, R. G. Weiss, *Chem. Commun.* **1996**, 2029.
27 J. van Esch, R. M. Kellogg, B. L. Feringa, *Tetrahedron Lett.* **1997**, *38*, 281.
28 K. Hanabusa, C. Koto, M. Kimura, H. Shirai, A. Kakehi, *Chem. Lett.* **1997**, 429.
29 M. Ikeda, M. Takeuchi, S. Shinkai, *Chem. Commun.* **2003**, 1354.
30 M. Shirakawa, N. Fujita, S. Shinkai, *J. Am. Chem. Soc.* **2003**, *125*, 9902.
31 K. Hanabusa, J. Tange, Y. Taguchi, T. Koyama, H. Shirai, *J. Chem. Soc., Chem. Commun.* **1993**, 390.
32 K. Hanabusa, M. Yamada, M. Kimura, H. Shirai, *Angew. Chem., Int. Ed. Engl.* **1996**, *35*, 1949.
33 K. Hanabusa, H. Kobayashi, M. Suzuki, M. Kimura, H. Shirai, *Colloid Polym. Sci.* **1998**, *276*, 252.
34 O. Wallach, *Justus Liebigs Ann. Chem.* **1895**, *286*, 90.
35 C. P. Brock, W. B. Schweizer, J. D. Dunitz, *J. Am. Chem. Soc.* **1991**, *113*, 9811.
36 C. M. Marson, I. Schwarz, *Tetrahedron Lett.* **2000**, *41*, 8999.
37 J. A. Lake, *Acta Crystallogr.* **1967**, *23*, 191.
38 D. Orthaber, A. Bergmann, O. Glatter, *J. Appl. Crystallogr.* **2000**, *33*, 218.
39 M. J. Taylor, S. Tanna, T. S. Sahota, B. Voermans, *Eur. J. Pharm. Biopharm.* **2006**, *62*, 94.
40 X.-F. Wei, R.-Y. Bao, Z.-Q. Cao, W. Yang, B.-H. Xie, M.-B. Yang, *Macromolecules* **2014**, *47*, 1439.
41 Y. Shi, M. Wang, C. Ma, Y. Wang, X. Li, G. Yu, *Nano Lett.* **2015**, *15*, 6276.
42 J. H. Jung, Y. Ono, K. Hanabusa, S. Shinkai, *J. Am. Chem. Soc.* **2000**, *122*, 5008.
43 O. Glatter, G. Fritz, H. Lindner, J. Brunner-Popela, R. Mittelbach, R. Strey, S. U. Egelhaaf, *Langmuir* **2000**, *16*, 8692.
44 O. Glatter, O. Kratky, *Small-Angle X-ray Scattering*, Academic, London, **1982**.
45 T. Sato, T. Akahane, K. Amano, R. Hyodo, K. Yanase, T. Ogura, *J. Phys. Chem. B* **2016**, *120*, 5444.
46 L. K. Shrestha, S. C. Sharma, T. Sato, O. Glatter, K. Aramaki, *J. Colloid Interface Sci.* **2007**, *316*, 815.
47 L. K. Shrestha, T. Sato, K. Aramaki, *Phys. Chem. Chem. Phys.* **2009**, *11*, 4251.
48 O. Glatter, *J. Appl. Crystallogr.* **1977**, *10*, 415.
49 O. Glatter, *J. Appl. Crystallogr.* **1980**, *13*, 577.
50 J. Brunner-Popela, O. Glatter, *J. Appl. Crystallogr.* **1997**, *30*, 431.
51 B. Weyerich, J. Brunner-Popela, O. Glatter, *J. Appl. Crystallogr.* **1999**, *32*, 197.
52 L. S. Ornstein, F. Zernicke, *Proc. K. Ned. Akad. Wet.* **1914**, *17*, 793.
53 S. H. Chen, *Annu. Rev. Phys. Chem.* **1986**, *37*, 351.
54 A. J. C. Wilson, *Arithmetic Crystal Classes and Symmophic Space Groups*, in *International Tables for Crystallography*, Kluwer Academic, London, **1992**, Vol. C, doi:10.1107/97809553602060000575.

